PREPRINT UCRL- 77415

Conf-760621--1

Lawrence Livermore Laboratory

FLOW THROUGH POROUS MEDIA FROM A NUCLEAR CAVITY

Frank A. Morrison, Jr.

October 17, 1975

This Paper was Prepared for Submission to
25th Heat & Fluid Mechanics Institute
University of California, Davis, Calif.; June 21-23, 1976

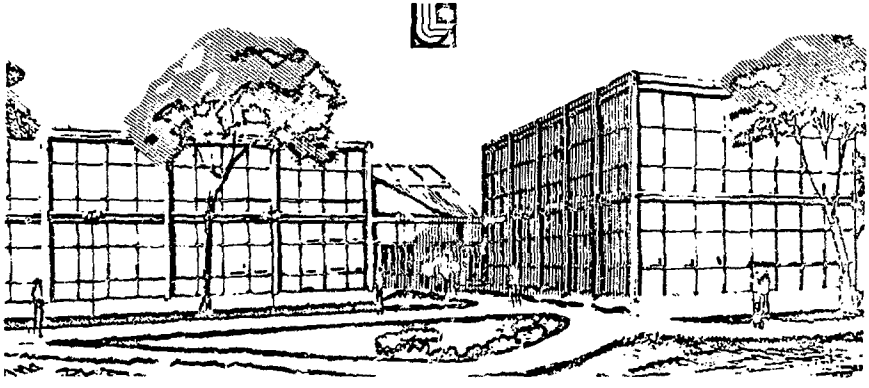

FLOW THROUGH POROUS MEDIA FROM A NUCLEAR CAVITY*

University of California

Frank A. Morrison, Jr.**

ABSTRACT

The transport of fluid from the cavity formed by an underground nuclear explosion is investigated. Driven by the high cavity pressure, steam and noncondensing gas enter the surrounding porous medium. Their subsequent motion through the medium is described and the extent of penetration determined. The relations governing the transport are presented. An implicit iterative computational method is developed. The relative merits of this technique are discussed. The method is applied to a nuclear test. Results of calculations are presented and discussed.

INTRODUCTION

Among the problems associated with the containment of underground nuclear tests is that of fluid flow from the nuclear cavity into the surrounding porous materials. *In the past several years, the testing community has devoted considerable* effort to developing an understanding of these flows and an ability to accurately and efficiently calculate the extent of such flow. Calculations of the predicted cavity fluid penetration have become part of the formal pre-shot containment evaluation. Such calculations are important in assessing such matters as depth of burial, stemming plans, and real estate conservation. Limits on acceptable penetration may also be imposed by such features as geological faults and neighboring emplacement holes.

The history of an underground cavity, following its formation, is described in detail by Kennedy and Higgins [1]. Cavity pressure measurements, from shortly after cessation of cavity growth until collapse, have also been reported [2]. For our purposes, we may consider the cavity to be originally filled with vapor at a pressure about the overburden pressure and a temperature of several thousand Kelvin. The vapor is primarily superheated steam. As a result of heat and mass transfer from the cavity, the pressure and temperature decay. The steam eventually begins to condense and the pressure drops more rapidly. The final stage is normally collapse of the cavity. The entire process occurs over a period ranging from a few minutes to over an hour.

Empirically predicted pressure and temperature histories for a proposed nuclear test are presented in Figs. 1 and 2. The primary object of this paper is to present a computational method permitting the efficient accurate calculation of flow from such a cavity into the surrounding medium.

*Work performed at and supported by the Lawrence Livermore Laboratory under the auspices of the U.S. Energy Research & Development Administration under contract No. W-7405-Eng-48.

**Professor of Mechanical Engineering, University of Illinois at Urbana-Champaign, Urbana, IL 61801

GOVERNING RELATIONS

The process is a transient, nonisothermal, two-phase, two-component flow. Superheated steam from the cavity is suddenly injected into a porous bed which is originally at ambient temperature. The void volume of this bed is initially occupied by air and any groundwater. Heat and mass transfer are coupled as heat is transferred to the bed and a condensation-evaporation mechanism strongly influences transport.

The two phases move at separate velocities. Air and water vapor travel together in a vapor mixture with an apparent velocity u_m. The liquid phase, occupied by water, has apparent velocity u_ℓ. Aside from the initial response quite near the cavity surface, these flows are characterized by low Reynolds numbers. Viscous drag dominates and the phase velocities are given by a form of Darcy's law appropriate to multiphase flow. For the vapor mixture,

$$u_m = - \frac{k_{rm}\, k}{\mu_m} \frac{\partial p}{\partial x} . \qquad (1)$$

$\partial p/\partial x$ is the local pressure gradient, μ_m is the vapor mixture viscosity, and k is the permeability of the bed. k_{rm} is the relative permeability which varies between zero and one and expresses the reduction in vapor mobility because of liquid in the pores. The absolute permeability, k, may vary with position, x. The relative permeability depends upon the saturation, S_m, the fraction of pore space occupied by vapor mixture. Liquid velocity obeys an equivalent relation obtained from Eq. (1) simply by replacing the subscript m by ℓ.

In addition to these constitutive equations describing phase velocities, the flow is governed by three conservation equations. These are mass conservation for each of the species and the first law of thermodynamics. Air continuity becomes

$$- \frac{\partial}{\partial x} (\rho_a\, u_m) = \epsilon \frac{\partial}{\partial t} (\rho_a\, S_m) \qquad (2)$$

while water continuity is

$$- \frac{\partial}{\partial x} (\rho_\ell\, u_\ell + \rho_v\, u_m) = \epsilon \frac{\partial}{\partial t} (\rho_\ell\, S_\ell + \rho_v\, S_m) \qquad (3)$$

ρ is the density and t, the time. Subscripts a and v denote air and water vapor, respectively. ϵ is the porosity, the void volume fraction of the bed. Porosity will vary with position.

Finally, with the assumption of local thermodynamic equilibrium, a control volume form of the first law is written for solid and fluids.

$$- \frac{\partial}{\partial x} (\rho_\ell u_\ell h_\ell + \rho_v u_m h_v + \rho_a u_m h_a) =$$

$$\varepsilon \frac{\partial}{\partial t} (\rho_\ell S_\ell e_\ell + \rho_v S_m e_v + \rho_a S_m e_a) + (1 - \varepsilon) \rho_s \frac{\partial e_s}{\partial t} \qquad (4)$$

h is the enthalpy per unit mass, e is the internal energy per unit mass and the subscript s denotes solid.

This model of the flow has been used by Morrison [3] in the analysis of a simpler flow using an explicit computational method. The assumptions and their justification are discussed in greater detail there. Laboratory experiments, analogous to the flow described in [3], have yielded results in excellent agreement with calculations [4].

COMPUTATIONAL METHOD

Calculations were performed on a uniform, one-dimensional Eulerian mesh. A node, denoted by the index i, is located a distance $(i - 1)\,\Delta x$ from the bed inlet. The temporal increment, which need not be held constant, is Δt. The index j denotes the time level.

TRANSPORT

The transport, described by the left-hand sides of Eqs. (2)-(4), is convective transport. The finite difference representation employs a windward or donor cell, e.g., see [5], differencing scheme. The method is transportive [6], i.e., calculated transport occurs only in the direction of the local velocity. The difference scheme also satisfies global conservation.

For flow from i - 1 to i to i + 1, the left-hand side of Eq. (2) becomes, for illustration,

$$- \frac{\partial}{\partial x} (\rho_a u_m) \simeq (\rho_{a,i-1} u_{m,i-\frac{1}{2}} - \rho_{a,i} u_{m,i+\frac{1}{2}})/\Delta x \qquad (5)$$

at node i. Extending a procedure developed by Runchal and Wolfshtein [7], we produce the more general expression

$$\begin{aligned} - \frac{\partial}{\partial x} (\rho_a u_m) \simeq [&\rho_{a,i-1} (u_{m,i-\frac{1}{2}} + |u_{m,i-\frac{1}{2}}|) \\ &- \rho_{a,i} (u_{m,i+\frac{1}{2}} + |u_{m,i+\frac{1}{2}}| - u_{m,i-\frac{1}{2}} + |u_{m,i-\frac{1}{2}}|) \\ &- \rho_{a,i+1} (u_{m,i+\frac{1}{2}} - |u_{m,i+\frac{1}{2}}|)]/2\Delta x \end{aligned} \qquad (6)$$

accounting for flow in either direction and for flow reversal. The finite difference approximation of the midpoint velocities follows from Eq. (1) and uses the node pressure at nodes adjacent to the midpoint.

Some numerical dispersion must result from using an Eulerian method. A Lagrangian approach was not adopted, however, because the flow is not characterized by a single fluid velocity.

IMPLICIT PROCEDURE

Several procedures, using expressions such as Eq. (6) and differing only in the time levels of the terms, can be developed. These procedures may have strikingly different characteristics. An explicit procedure calculates the fluxes using values at the old time level (j) in order to determine properties at the new time level ($j + 1$). Such a method is certainly the easiest to develop and was employed in [3]. In practice, however, a time step limitation, imposed by a stability criterion characteristic of the method, severely restricted its utility. A method free of this restriction was needed.

The method finally produced was inspired by the work of Evans, Brousseau, and Keirstead [8] on the stability of finite difference approximations to the diffusion equation. While their stable iterative methods have not been widely used to solve the diffusion equation, these methods to possess attractive characteristics that recommend their adaptation to problems as are treated here.

To illustrate the characteristics, let us examine a few numerical techniques for solution of the diffusion equation.

$$\frac{\partial^2 c}{\partial x^2} = \frac{\partial c}{\partial t} \tag{7}$$

Because of the importance and linearity of Eq. (7), much is known about its solution. This provides valuable guidance in developing methods for our related nonlinear equations.

The explicit approximation

$$\frac{c_{i+1}^j - 2c_i^j + c_{i-1}^j}{(\Delta x)^2} = \frac{c_i^{j+1} - c_i^j}{\Delta t} \tag{8}$$

to the diffusion equation is the simplest method. The truncation error is of order Δt, $(\Delta x)^2$. The disadvantage of this approach is the restriction

$$\frac{\Delta t}{(\Delta x)^2} \leq \frac{1}{2} \tag{9}$$

for stability. Adaptation to the multiphase flow calculation requires solution of the finite difference equivalents of Eqs. (2)-(4) for local air mass, water mass, and energy, respectively. These properties, together with state relations, are subsequently used to find the local thermodynamic state. The solution technique depends upon the water phases present. The time step is limited in a manner similar to Eq. (9).

The normal implicit method of solving the diffusion equation is obtained by evaluating spatial derivatives (fluxes) at the new (j + 1) time level.

$$\frac{c_{i+1}^{j+1} - 2c_i^{j+1} + c_{i-1}^{j+1}}{(\Delta x)^2} = \frac{c_i^{j+1} - c_i^j}{\Delta t} \qquad (10)$$

This form has the same truncation error as the explicit form, but is unconditionally stable. The size of the time step is restricted only by requirements of accuracy. Unknown (j + 1 level) values at three spatial locations appear in Eq. (10). Consequently, values at the j + 1 time level are found by the solution of a set of finite difference equations with a tridiagonal coefficient matrix. An efficient algorithm [9] for the solution of a tridiagonal set of n equations is available and requires only 5n - 2 storage locations and a number of operations of order n.

The extension of this implicit approach to multiphase flow calculations would remove the stability limit but coupling unknowns at different nodes introduces other objectionable features. Because the multiphase flow equations are coupled and since new time level properties at three nodes would appear, the bandwidth would be at least nine. The actual width would depend on the state relations and the amount of solution done by the programmer. The solution of these equations is considerably more costly and time consuming than the solution of tridiagonal sets. Further, the equations to be solved depend upon the phases present at each of the nodes. Finally, since the conservation equations are nonlinear, iteration should be necessary.

The iterative schemes of Evans, Brousseau, and Keirstead present an opportunity to perform unconditionally stable calculations while avoiding the inversion of large bandwidth matrices. Of these methods, we consider one that reduces to the form

$$\frac{c_{i+1}^{j+1,p} - 2c_i^{j+1,p+1} + c_{i-1}^{j+1,p}}{(\Delta x)^2} = \frac{c_i^{j+1,p+1} - c_i^j}{\Delta t} \qquad (11)$$

The superscript p is an iteration index. Values are known for iteration level p and sought at level p + 1. The zeroeth iteration corresponds to values at the old (j) time level. Note that only the unknown at node i appears. The solution does not require simultaneous solution at all nodes. While the method is iterative, the adaptation to nonlinear problems would be iterative in any event.

The convergence rate of the iteration may be improved by using the most recent values from the neighboring nodes. For a calculation proceeding in the direction of increasing i, the relation

$$\frac{c_{i+1}^{j+1,p} - 2c_i^{j+1,p+1} + c_{i-1}^{j+1,p+1}}{(\Delta x)^2} = \frac{c_i^{j+1,p+1} - c_i^j}{\Delta t} \qquad (12)$$

should converge faster than Eq. (11) while introducing no additional labor.

Air continuity provides a simple relation to demonstrate application of the method to flow. Consider the case when water is superheated. The mixture saturation and relative permeability are each unity. Equation (1) is substituted into Eq. (2) and the result reduces to

$$\frac{\partial}{\partial x}\left(\rho_a \frac{k}{\mu_m}\frac{\partial p}{\partial x}\right) = \varepsilon \frac{\partial \rho_a}{\partial t} . \qquad (13)$$

The finite difference form is produced as follows. Windward differencing is employed. Permeability, k_i, is the effective permeability in the range i to i + 1. ε_i is the average porosity in the cell surrounding node i. No iteration is performed on transport properties. These are evaluated at the old time level. Iteration is done on all thermodynamic properties. Most recent values are used for thermodynamic properties.

The nonlinearity produces a product of unknown density and pressure which is removed by linearizing between iterations.

$$\rho_{a,i}^{j+1,p+1}\; p_i^{j+1,p+1} \simeq \rho_{a,i}^{j+1,p+1}\; p_i^{j+1,p} + \rho_{a,i}^{j+1,p}\; p_i^{j+1,p+1} - \rho_{a,i}^{j+1,p}\; p_i^{j+1,p} \qquad (14)$$

A product of the density difference and pressure difference is discarded.

For flow in the direction of increasing x and calculations proceeding in the same direction, the finite difference form of Eq. (13) reduces to

$$\frac{k_i}{\mu_i^j}\left[\rho_{a,i}^{j+1,p+1}\,(p_{i+1}^{j+1,p} - p_i^{j+1,p}) - \rho_{a,i}^{j+1,p}\,(p_i^{j+1,p+1} - p_i^{j+1,p})\right]$$

$$- \frac{k_{i-1}}{\mu_{i-1}^j}\left[\rho_{a,i-1}^{j+1,p+1}\,(p_i^{j+1,p+1} - p_{i-1}^{j+1,p+1})\right] = \frac{\varepsilon_i\,(\Delta x)^2}{\Delta t}\,(\rho_{a,i}^{j+1,p+1} - \rho_{a,i}^{j}) \qquad (15)$$

A computer program, CERBERUS, that uses this approach has been written. Equations, equivalent to Eq. (15) but accounting for flow reversal, were developed for air and water continuity and the first law of thermodynamics. These, together with state relations, are solved to determine the thermodynamic state at each node i.

Results of calculations with CERBERUS are presented in the next section. It is worthwhile here to compare the computer time required for that run with the time requirements of an alternative explicit calculation. A bed with 400 nodes was used. At each time step, however, calculations were performed for fewer nodes. Starting at the cavity, calculations were done at each node until the local pressure differed from ambient pressure by less than about a pascal at four successive nodes. The time step was chosen to be 1 second and 10 iterations were done at each time step. The resulting calculation, for two hours of real time, required 11.6 minutes of machine time on a CDC 7600. Experience with the explicit program indicates that the equivalent 400 node explicit calculation with pressure test would require an estimated day of machine time.

Further savings can be obtained with better parameter choices for the implicit calculation. The example choices are by no means optimal. In particular, ten iterations is quite excessive.

RESULTS OF CALCULATIONS

The example is based on a proposed experiment at the Nevada Test Site. The anticipated cavity pressure and temperature histories are shown in Figs. 1 and 2. The cavity contains steam. The distance between the predicted cavity ceiling and ground surface is 1,140 metres. The emplacement hole is stemmed. Figure 3 shows that portion of a proposed stemming plan lying above the cavity ceiling. As a prudent measure, plugs are ignored and are not presumed to contain any flow. The emplacement hole is cased and should be dry.

The pressure distribution in the stemming was calculated using CERBERUS and is shown in Fig. 4 for several selected times after the detonation. The coupled water saturation distribution at the same times is shown in Fig. 5.

The 10-, 20-, and 40-minute curves are characteristic of the early response and closely resemble the similarity solution of Morrison [3]. Features in Figs. 4 and 5 are related and should be compared. A saturation region is passing through the column. The column ahead of the saturation front contains air at ambient temperature and low pressure. As the front passes, the column becomes warmer and the saturation pressure increases. Water, as liquid and vapor, displaces the air. Behind the liquid is a region of dry superheated steam. The liquid transport is accomplished primarily by evaporation and condensation.

The 80-minute curves exhibit some features of late time behavior. Figures 6 and 7, showing properties two hours after detonation, show these more clearly. The cavity pressure boundary condition has dropped to ambient. The pressure within the column remains higher. The high column pressure is produced by vaporization of liquid in the high temperature portion of the saturated region. This will continue until no liquid remains at temperatures greater than the saturation temperature at ambient pressure.

The displacement of air by the steam is seen in Fig. 6. The dotted line shows the partial pressure of the water vapor. Nearer the cavity, the total pressure is exerted by the water vapor. Farther from the cavity, the partial pressure of air dominates. The slight mixing results from numerical dispersion but remains acceptably small.

The penetration of cavity fluid into the column can be determined here by the position of the saturation front. The extent of penetration is crucial in containment evaluation. The progress of the saturation front is shown in Fig. 8.

DISCUSSION

The flow from a nuclear cavity has been described. A stable iterative numerical technique has been devised to calculate such flow. The resulting program, CERBERUS, is over two orders of magnitude faster than the corresponding explicit program. This increased speed permits the routine calculation of these flows in detail. Results of one such calculation were presented and the advance of the cavity fluid determined.

NOMENCLATURE

c = diffused quantity

e = internal energy per unit mass

h = enthalpy per unit mass

k = permeability

k_r = relative permeability

p = pressure

S = saturation

t = time

u = apparent speed

x = position

ϵ = porosity

μ = viscosity

ρ = density

Subscripts

a = air

i = spatial index

ℓ = liquid

m = mixture

s = solid

v = water vapor

Superscripts

j = temporal index

p = iteration index

REFERENCES

1. Kennedy, G. C. and G. H. Higgins, Temperatures and pressures associated with the cavity produced by the Rainier event, UCRL-5281, 1958.

2. Olsen, C. W., Time history of the cavity pressure and temperature following a nuclear detonation in alluvium, J. Geophys. Res., 1967, 72, 5037-5041.

3. Morrison, Frank A., Jr., Transient multiphase multicomponent flow in porous media, Int. J. Heat Mass Transfer, 1973, 16, 2331-2342.

4. Pitts, J. H., private communication.

5. Gentry, R. A., R. E. Martin, and B. J. Daly, An Eulerian differencing method for unsteady compressible flow problems, J. Comp. Physics, 1966, 1, 87-118.

6. Roache, P. J., Computational Fluid Dynamics, Hermosa Publishers, Albuquerque, 1972.

7. Runchal, A. K. and M. Wolfshtein, Numerical integration procedure for the steady state Navier-Stokes equations, J. Mech. Engr. Sci., 1969, 11, 445-453.

8. Evans, G. W., R. J. Brousseau, and R. Keirstead, Instability considerations for various difference equations derived from the diffusion equation, UCRL-4476, 1954.

9. Hornbeck, J. W., Numerical Marching Techniques for Fluid Flows with Heat Transfer, NASA SAP-297, 1973.

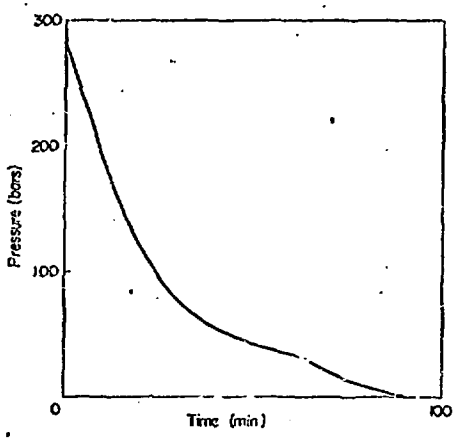

Fig. 1 Cavity pressure history

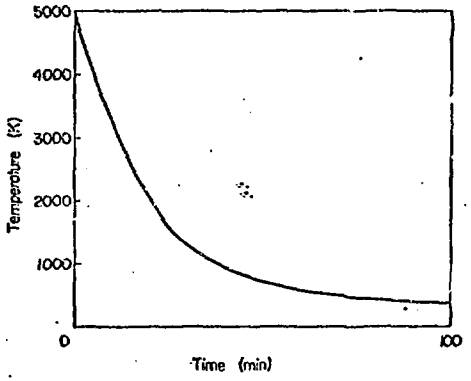

Fig. 2 Cavity temperature history

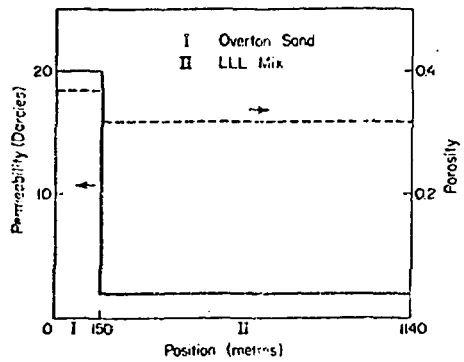

Fig. 3 Stemming in region above cavity
(1 Darcy = 9.8 x 10^{-13} m^2)

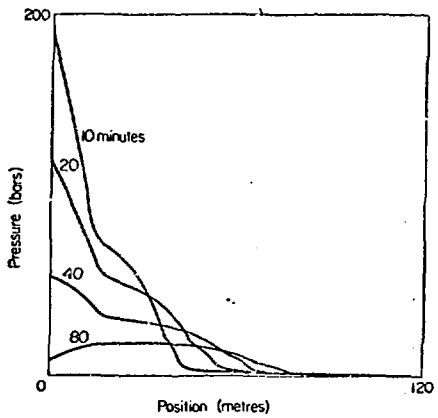

Fig. 4 Pressure in column above cavity

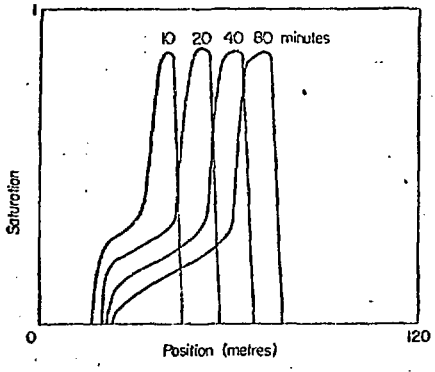

Fig. 5 Water saturation in column above cavity

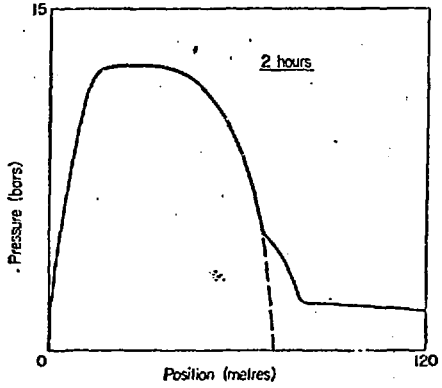

Fig. 6 Pressure in column after 2 hours. Solid line is total pressure; dashed line is partial pressure of water vapor.

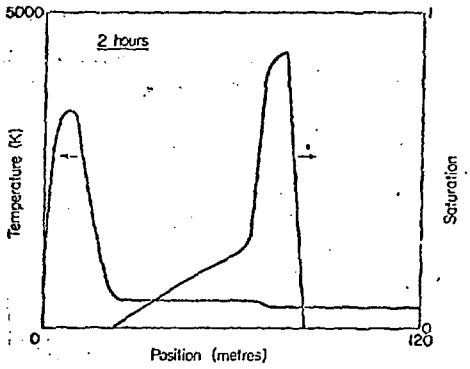

Fig. 7 Temperature and saturation in column

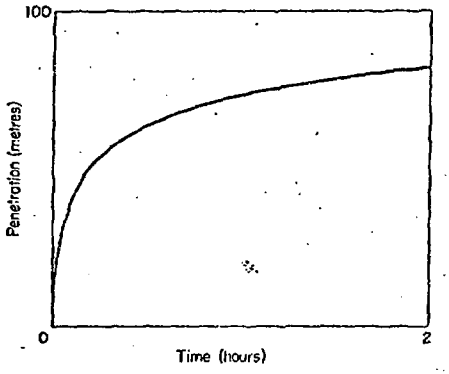

Fig. 8 Penetration of cavity fluid